Contribution of astrophysical events to the chemical evolution of a dwarf irregular galaxy

Nao Fukagawa, Nikos Prantzos

Monthly Notices of the ROYAL ASTRONOMICAL SOCIETY

MNRAS **534,** 2006–2013 (2024) https://doi.org/10.1093/mnras/stae2210
Advance Access publication 2024 September 24

Contribution of astrophysical events to the chemical evolution of a dwarf irregular galaxy

Nao Fukagawa[1,2]★ and Nikos Prantzos[3]

[1]*Department of Astronomical Science, School of Physical Sciences, The Graduate University for Advanced Studies, SOKENDAI, 2-21-1 Osawa, Mitaka, Tokyo 181-8588, Japan*
[2]*National Astronomical Observatory of Japan, 2-21-1 Osawa, Mitaka, Tokyo 181-8588, Japan*
[3]*Institut d'Astrophysique de Paris, CNRS and Sorbonne Université, 98bis Bd. Arago, 75014 Paris, France*

Accepted 2024 September 18. Received 2024 August 28; in original form 2024 June 6

ABSTRACT

We study the contribution of various astrophysical events asymptotic giant branch (AGB stars, core collapse and thermonuclear supernovae, neutron star mergers, and collapsars) to the abundances of elements both up to and heavier than the iron peak in a Local Group dwarf irregular galaxy, Wolf–Lundmark–Melotte (WLM). Its star formation history has been recently determined by observations with the *JWST*, and we use it to estimate the occurrence of the astrophysical sources. The rates of the gas accretion and the outflow are roughly determined based on the stellar metallicity distribution, the oxygen abundance of H II regions, and the gas fraction. As discussed in the literature, the difference in time-scales on which the astrophysical events release the nucleosynthesis products is seen in the occurrence of the events and the evolution of abundance ratios. WLM has an extended star formation history and massive stars are recently and currently formed. Thus, the contribution of rotating massive stars through the weak s-process appears in the abundance ratios of light trans-iron elements to iron at later time of the evolution.

Key words: galaxies: dwarf – galaxies: evolution – nuclear reactions, nucleosynthesis, abundances – stars: abundances – ISM: abundances.

1 INTRODUCTION

The chemical abundances measured for individual stars and gas in Local Group dwarf galaxies bring understanding on the astrophysical sources of different elements in low-metallicity systems. Owing to deep photometry with ground-based and space telescopes, the star formation history in the early phase of the evolution of nearby dwarf galaxies is recovered (e.g. McQuinn et al. 2024, and references therein), which can be a hint on the chemical evolution of individual dwarf galaxies.

Astrophysical events release nucleosynthesis products on different time-scales. More massive stars tend to have shorter lifetimes, while low-mass stars, Type-Ia supernovae (SNe Ia), and neutron star mergers (NSMs) can enrich the surroundings on long time-scales. The difference in time-scales may be reflected in abundance ratios (e.g. Tinsley 1979; Gilmore & Wyse 1991). If star formation episodes are separated by quiescent periods of low star formation rates, the impact of individual events and the variation of the star formation rate might appear on the chemical abundance.

Wolf–Lundmark–Melotte (WLM) is a Local Group barred dwarf irregular galaxy (dIrr) located at about 932 and 836 kpc away from the Milky Way and M31, respectively (e.g. McConnachie 2012, references therein). The distance from the nearest galaxy is about 175 kpc (Cetus dwarf spheroidal galaxy, Whiting; Hau & Irwin 1999). According to the distribution of H I gas, there is no clear evidence for recent merger or interaction with other systems (e.g. Jackson et al. 2004). Thus, WLM is one of the most isolated dIrrs in the Local Group and provides insights into the effects of stellar feedback and secular processes on the evolution of low-mass galaxies (e.g. Leaman et al. 2012). The chemical abundances have been measured for individual stars as well as ionized gas associated with H II regions (see Section 2).

Numerical simulations, semi-analytical models, and simple models are all essential to discuss the chemical evolution (e.g. Matteucci 2021; Diehl & Prantzos 2023, for reviews). While observed quantities may not be completely reproduced due to the small number of assumptions, simple models are useful to observe the variation of the properties of galaxies with physical quantities. With a simple model where stochasticity is introduced into the occurrence of astrophysical events as rarity, we discuss the contribution of astrophysical events to the chemical evolution in WLM. The observational data are summarized in Section 2. In Section 3, we estimate the number of astrophysical events with the star formation history derived from the colour–magnitude diagram. The chemical evolution model and the assumptions are described in Section 4. The global properties and the evolution of abundance ratios are discussed in Sections 5 and 6, respectively.

2 OBSERVATIONAL DATA

The observational data are gathered from the literature. We focus on a region on the bar for which the star formation history has been derived.

★ E-mail: naofukagawa@gmail.com

The gas fraction defined as $f_g = \frac{M_g}{M_g+M_*}$ is estimated from the gas mass $M_g(M_\odot)$ and the stellar mass $M_*(M_\odot)$. For the latter, the stellar mass of WLM is estimated to be $M_* \sim 4 \times 10^7\,M_\odot$ (e.g. Woo, Courteau & Dekel 2008; McConnachie 2012). The H I gas mass of WLM is almost comparable to the stellar mass ($M_{HI} \sim 3 \times 10^7$ to $\sim 10^8\,M_\odot$; e.g. Barnes & de Blok 2004; Jackson et al. 2004; Kepley et al. 2007). The gas fraction ($f_g \sim 0.6$) is derived by assuming that H I gas dominates the mass of the interstellar gas and considered to be the average in the region on the bar. We note that stars and H I gas may not uniformly distribute in WLM. In addition, the detection of carbon monoxide (e.g. Elmegreen et al. 2013) and the analysis of the rotation curve (Jackson et al. 2004; Leaman et al. 2012) suggest the presence of molecular gas. Thus, the derived gas fraction should be regarded as a typical value.

The oxygen abundance of H II regions in WLM is about 7–13 per cent of the solar abundance (e.g. Skillman, Terlevich & Melnick 1989), depending on the measurement and the adopted solar value. We refer to the oxygen abundance and the N/O ratio of two H II regions in the bar measured by Lee, Skillman & Venn (2005).

The average oxygen abundance of supergiants in WLM is comparable to that of H II regions (Bresolin et al. 2006), while there may be spatial inhomogeneity in the chemical abundance (Venn et al. 2003; Lee et al. 2005). The abundance of 12 elements of a supergiant in the bar (WLM-15) has been measured by Venn et al. (2003). This star may have a metallicity ([Z]) higher than the average of supergiants in WLM (Urbaneja et al. 2008).

The metallicity distribution of a field on the bar has been derived by Leaman et al. (2009). The distribution includes 44 red giant branch stars, and the average metallicity of the stars is [Fe/H][1] $= -1.14 \pm 0.04$. The metallicity distribution has a peak at [Fe/H] ~ -1.3.

The star formation history of WLM has been inferred based on the colour–magnitude diagram[2] (e.g. Tosi, Greggio & Focardi 1989; Dolphin 2000; Albers et al. 2019). We refer to the star formation history in a region on the bar derived by McQuinn et al. (2024).

3 OCCURRENCE OF ASTROPHYSICAL SOURCES

Fig. 1(a) shows the time variation of the star formation rate based on the cumulative star formation history derived by McQuinn et al. (2024). In the early phase of the evolution, there seems to be star formation episodes separated by quiescent periods of low star formation rates. For the last several Gyrs, the star formation continues with increases and decreases.

Based on the star formation history, we estimate the number of astrophysical sources in a time-step. The definition of the number of events, the concept of rare events, and the assumptions about astrophysical sources are the same as those in Fukagawa & Prantzos (2023, hereafter FP23). Below is a brief summary.

We include massive stars ($M > 10\,M_\odot$), low- and intermediate-mass stars (LIMS, $M < 10\,M_\odot$), SNIa, and candidates for the rapid (r-) neutron capture process in the source of the chemical enrichment. Massive stars of 10–25 and 25–120 $M_\odot$ are assumed to evolve into core-collapse supernovae (CCSNe) and black holes, respectively. Each star formed at time t of mass M is assumed to release the material at $t + \tau_M$, where τ_M denotes the lifetime of the star of mass M derived based on stellar evolution models (Schaller et al. 1992).

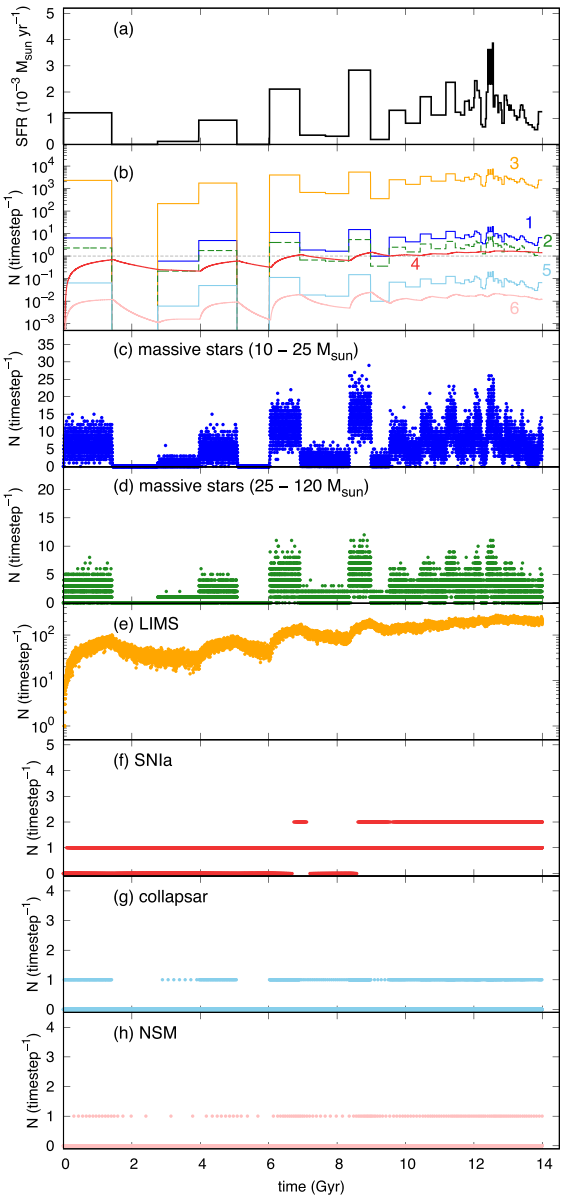

Figure 1. Time variation of the star formation rate in the region on the bar of WLM (panel a), the number of events when the rarity is not introduced (panel b), and the number of dying stars, SNIa, and the r-process events when the rarity is introduced (panels c–h). The star formation rate in panel (a) is based on the cumulative star formation history derived by McQuinn et al. (2024). Curves in panel (b) correspond to the number of the astrophysical sources in a time-step: massive stars that evolve into CCSNe (10–25 $M_\odot$, curve 1 in blue), massive stars that evolve into black holes (25–120 $M_\odot$, broken curve 2 in green), LIMS (curve 3 in orange), SNIa (curve 4 in red), collapsar (curve 5 in light blue), and NSM (curve 6 in pink), respectively. In the panel, we show the number of stars formed in each time-step.

[1]Hereafter, metallicity represents the abundance of iron, if not otherwise specified. For the abundance ratio, [A/B] $= \log(N_A/N_B) - \log(N_A/N_B)_\odot$, where N_A and N_B denote the abundance of A and B.

[2]While stars can migrate in a galaxy, the star formation history is generally derived based on the colour–magnitude diagram that includes stars currently observed in a field. Nevertheless, the observationally derived star formation rate in the past brings understanding on the evolution of individual dwarf galaxies that may not always follow the star formation law for local spiral galaxies (e.g. de los Reyes & Kennicutt 2019).

Table 1. The number of astrophysical sources in unit mass ($n_{\rm event}$)[a] and the total number of the astrophysical sources throughout the evolution in the region.

	$n_{\rm event}$	Total number
Total mass of stars ($M_\odot$)	–	1.3×10^7
Massive star (10–25 $M_\odot$)	5.3×10^{-3}	70 670
Massive star (25–120 $M_\odot$)	1.9×10^{-3}	25 334
LIMS	1.9	2533 4558
SNIa	1.3×10^{-3}	11 746
NSM	1.2×10^{-5}	143
Collapsar	5.3×10^{-5}	706

Note. The total mass of stars formed in the region is taken from McQuinn et al. (2024). For massive stars and LIMS, the number of stars formed in the region is shown. [a]For SNIa and NSM, the number in unit mass shown in this table is derived by integrating the delay-time distributions.

For the r-process, we consider NSM and collapsar to be the dominant sites. We note that astrophysical sites of the r-process are actively discussed as summarized in FP23.

The number of stars formed in a time-step is derived by $N_{\rm event}(t) = \Psi(t)\,\Delta t\, n_{\rm event}$, where $\Psi(t)$ and Δt denote the star formation rate and the time-step. We adopt $\Delta t = 10^{-3}$ Gyr by considering mass ejection from massive stars and precision in the calculations. The number of stars in unit mass ($n_{\rm event}$) is estimated by adopting the stellar initial mass function (IMF) in the solar neighbourhood (Kroupa 2002). The number of SNIa and that of NSM are estimated by $N_{\rm event} = R(t)\,\Delta t$, where $R(t)$ is the rate of SNIa or NSM derived from the delay-time distributions (DTDs). For SNIa, we adopt the DTD $\propto t^{-1}$ (e.g. Maoz & Graur 2017, and references therein) and the formula by Greggio (2005) at early times. For NSM, we refer to the DTD by Beniamini & Piran (2019). The occurrence of collapsar is assumed to be 1 per cent of that of CCSNe (e.g. MacFadyen & Woosley 1999). When the number of an astrophysical source in a time-step is less than unity ($N_{\rm event} < 1$), we consider the event to be rare and introduce stochasticity into the occurrence of the astrophysical source. Table 1 summarizes the total number of the astrophysical events.

Fig. 1(b) shows the number of each astrophysical source in a time-step before the rarity is introduced. The time variation of the number of stars formed in a time-step shows similar trends to that of the star formation rate. Regarding SNIa and NSM, the progenitors (white dwarfs and neutron stars, respectively) require time to reach the explosive events. Thus, the time variation of the number of SNIa and NSM is more smooth than that of stars. According to the concept of rarity, massive stars can be rare when the star formation rate is low. Due to the low occurrence, the r-process candidates are rare throughout the evolution of WLM.

Figs 1(c), (d), and (e) show the number of dying massive stars (CCSNe and black holes) and LIMS when the rarity is introduced. Since more massive stars tend to have shorter lifetimes, the time variation of the number of dying massive stars follows that of the star formation rate. The dispersion in the number of dying massive stars is due to the different lifetimes and the rarity. On the other hand, less massive stars are more numerous and tend to have longer lifetimes. Except for the early time, over ten dying LIMS can appear in a time-step even when the star formation rate gets low (Fig. 1(e)).

SNIa is rare at the early time (Fig. 1(f)). Similar to dying LIMS, SNe Ia appear when the star formation rate is low.

With regard to the r-process candidates, collapsars, and NSMs can appear in star formation episodes. NSMs can also occur after or between star formation episodes.

4 CHEMICAL EVOLUTION MODEL

The variation of the star formation rate and the properties of dIrrs have been discussed in the literature. For instance, with regard to the stochastic star formation, Gerola, Seiden & Schulman (1980, and references therein) have investigated the properties, such as star formation rate, colours, luminosity, and metallicity, of galaxies of different sizes by introducing stochasticity into the propagation of star formation. The stochastic self propagation of star formation has been incorporated into chemical evolution models (e.g. Matteucci & Chiosi 1983).

Concerning the star formation history, based on calculations of the colour of galaxies, Searle, Sargent & Bagnuolo (1973) have suggested that the star formation of blue compact dwarf galaxies is discontinuous. Generally, star formation in dIrrs tends to be more moderate and separated by shorter intervals (e.g. Marconi et al. 1995). The impact of bursts on abundance ratios has been investigated (e.g. Gilmore & Wyse 1991; Bradamante, Matteucci & D'Ercole 1998).

Also, along with the idea that H II regions are enriched in nucleosynthesis products released by massive stars on short time-scales (e.g. Kunth & Sargent 1986), Pilyugin (1992) has investigated the evolution of the N/O ratio with the model where stars enrich giant H II regions during star formation episodes and the gas is mixed throughout the galaxy in the subsequent quiescent periods. Since massive stars produce oxygen in H II regions and LIMS produce nitrogen on longer time-scales, the N/O ratio evolves in a zig-zag manner.

In the present study, we introduce stochasticity into the occurrence of each astrophysical source in a quantitative way. We also include the contribution of rotating massive stars to the chemical evolution through the slow (s-) neutron capture process (the weak s-process).

We assume that there is no gas or star at the beginning in the region and that the chemical evolution proceeds through the gas accretion, the star formation, and the outflow.

In general, the movement of gas in bars is complex (e.g. Athanassoula 1992). Galaxies can acquire the material to form stars through the gas accretion. Also, the gas accretion may induce the star formation through the compression of the interstellar medium. According to numerical simulations (e.g. Muratov et al. 2015), the star formation rate tends to increase when or after the rate of the gas accretion increases.

In the meanwhile, the variation of the rate of the gas accretion in star formation episodes and that in quiescent periods are not clear. One of the interpretations of starbursts associated with low-metallicity gas in dwarf galaxies is the accretion of metal-poor gas (e.g. Sánchez Almeida et al. 2015). At the same time, stellar feedback can decrease the rate of the gas accretion due to the interaction between the accreting gas and the interstellar gas expelled from star-forming regions (e.g. van de Voort 2017, for a review). In the present study, we simply assume that the metal-free gas accretes on to the region at the rate $F(t) \propto \exp(-\alpha\, t)$, where α(Gyr^{-1}) is a constant referred to as the time-scale of the gas accretion.

Astrophysical events appear along the number of the sources estimated in Section 3. For each star, the mass is randomly given along the IMF (Kroupa 2002), and the metallicity is given based on that of the interstellar gas. The initial rotational velocity of individual massive stars is randomly determined along the initial distribution of rotational velocity proposed in Prantzos et al. (2018).

In the model, the star formation rate at a given time is determined by the total mass of stars formed in a time-step. Thus, the modelled star formation rate is expected to depend on the number of stars

Table 2. Summary of the efficiency of the outflow (k) and the time-scale of the gas accretion (α Gyr^{-1}).

k, α(Gyr^{-1})	$k = 1.1 \times 10^3$, $\alpha = 0.05$–0.06
	$k = 1.2 \times 10^3$, $\alpha = 0.05$–0.07
	$k = 1.3 \times 10^3$, $\alpha = 0.05$–0.06
typical k, α(Gyr^{-1})	$k = 1.2 \times 10^3$, $\alpha = 0.06$

formed in a time-step and the observationally derived star formation history.

We assume that part of the interstellar gas is expelled from the region due to CCSNe. The outflow rate is assumed to be proportional to the number of CCSNe in a time-step and given by $O(t) \propto \frac{k\,N_{\rm CCSN}}{\Delta}\,t$, where k is a constant referred to as the efficiency of the outflow. We note that gas heating might play an important role on the star formation, the gas accretion, and the outflow as discussed in McQuinn et al. (2024). Also, if a dwarf galaxy has an active galactic nucleus, the evolution of the host galaxy might be influenced.

The metallicity distribution reflects the star formation, the gas accretion and the outflow (e.g. Lynden-Bell 1975; Hartwick 1976). Also, the average metallicity at a given gas fraction can decrease due to outflow induced by supernovae (e.g. Larson 1974; Matteucci & Chiosi 1983). By comparing the metallicity distributions, the oxygen abundance of H II regions and the gas fraction to those predicted by the model, the efficiency of the outflow and the time-scale of the gas accretion are roughly determined (Table 2).

We refer to the chemical evolution model described in FP23 and take into account the presence of gas in WLM at the present universe.[3] With regard to the source of the chemical enrichment, we include massive stars of different initial rotational velocities, and stellar yields provided by Limongi & Chieffi (2018) are adopted. In the nucleosynthesis calculations, stars of $M < 25\,{\rm M}_\odot$ evolve into CCSNe and release the nucleosynthesis products through the stellar wind and the supernova explosion. More massive stars ($M > 25\,{\rm M}_\odot$) evolve into black holes and contribute to the chemical enrichment through the stellar wind. The mixing and fallback process (Umeda & Nomoto 2002) is also taken into account. We assume the initial distribution of rotational velocities by Prantzos et al. (2018). For LIMS, stellar yields by Cristallo et al. (2015) are adopted. Regarding SNIa, the mechanism of the explosion and the yields at low metallicities are under discussion. In the present study, we adopt the yield by Iwamoto et al. (1999). Since yields for the r-process candidates can depend on the properties of the progenitors, we assume that the abundance pattern of yields for NSM ($Y_{i,\rm NSM}$) and collapsar ($Y_{i,\rm col}$) is consistent with the solar r-process component: $Y_{i,\rm NSM} \propto (1 - A_{\rm r}) \cdot (X_{i,\odot}\, f_{i,\rm r})$ and $Y_{i,\rm col} \propto A_{\rm r} \cdot (X_{i,\odot}\, f_{i,\rm r})$, where $X_{i,\odot}$ and $f_{i,\rm r}$ are the solar abundance of element i (Lodders, Palme & Gail 2009) and the solar r-component (Prantzos et al. 2020), respectively. $A_{\rm r}$ is the relative contribution of the r-process sites and tentatively set to be $A_{\rm r} = 0.5$. The assumptions about the r-process candidates and the yields are described in FP23.

5 GLOBAL PROPERTIES

We investigate the time variation of global properties predicted by the model when the typical values of the efficiency of the outflow and the time-scale of the gas accretion (Table 2) are adopted.

[3]While the distribution of stars and gas may not be uniform, we roughly estimate the present-day gas mass of the region based on the gas fraction.

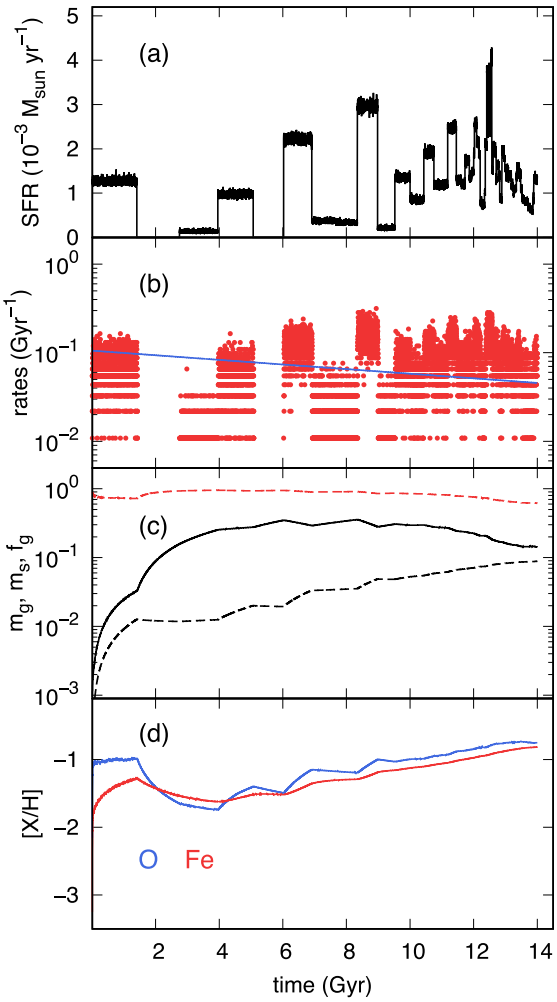

Figure 2. Time variation of physical quantities predicted by the model when the typical values of the efficiency of the outflow and the time-scale of the gas accretion are adopted ($k = 1.2 \times 10^3$ and $\alpha = 0.06$ Gyr^{-1}). (a) The star formation rate in the model. (b) The rate of the gas accretion (blue curve) and that of the outflow (red dots). (c) The mass fraction of gas (black solid curve) and that of stars (black dotted curve) in the region. The red dotted curve shows the gas fraction ($f_{\rm g}$). (d) The abundance of oxygen (blue curve) and that of iron (red curve), respectively. Quantities shown in panels (b) and (c) are scaled to the total mass accreted on to the region.

Fig. 2(a) shows the time variation of the star formation rate in the region. The modelled star formation rate is derived from the total mass of stars formed in a time-step, and the time variation follows that of the observationally derived star formation rate. Since each star has its own mass, the modelled star formation rate oscillates.

The rate of the gas accretion and that of the outflow are shown in Fig. 2(b). In the model, the gas continuously accretes on to the region. Since the outflow is induced by CCSNe, the time variation of the outflow rate reflects that of the star formation rate.

Fig. 2(c) shows the gas mass and the stellar mass scaled to the total mass of gas that accretes on to the region. The mass of gas in the region increases at the early time due to the gas accretion, while the gas is consumed by the star formation and the outflow. Each star formation episode increases the stellar mass. The gas acquisition and consumption are reflected in the variation of the gas fraction ($f_{\rm g}$).

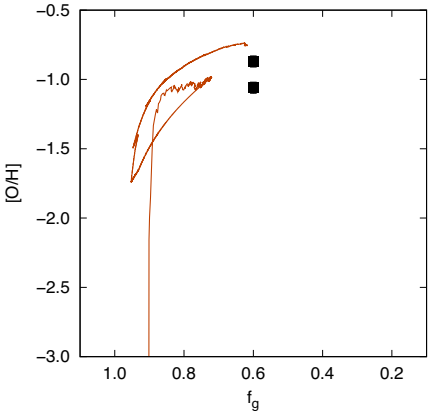

Figure 3. The evolution of the oxygen abundance and the gas fraction. The black squares show the oxygen abundance of two H II regions measured by Lee et al. (2005) and the average gas fraction of WLM. The orange curve shows the evolution of the oxygen abundance and the gas fraction predicted by the model.

Fig. 2(d) shows the time variation of the abundance of oxygen and that of iron.[4] Oxygen is produced mainly by massive stars. A large number of massive stars increase the oxygen abundance to [O/H] ~ -1 in the first star formation episode. When the star formation rate is low, the number of massive stars formed in a time-step decreases. Also, the interstellar medium is diluted with the accreting gas. Thus, the oxygen abundance temporarily decreases in quiescent periods. At the later time, the oxygen abundance generally increases with time.

In the model, iron is produced by massive stars and SNe Ia. Since white dwarfs reach SNe Ia certain time after the formation, the iron abundance can increase even in quiescent periods. Thus, the decrease in the iron abundance in quiescent periods is modest compared to that in the oxygen abundance. At the present universe, the iron abundance in the interstellar medium can be as high as the oxygen abundance.

The time variation of the oxygen abundance and that of the gas fraction are reflected in the evolution of the model predictions on the [O/H] – f_g plane (Fig. 3). Until around the end of the first star formation episode, the oxygen abundance reaches [O/H] ~ -1, and the gas fraction decreases to $f_g \sim 0.7$. In the subsequent quiescent period, the gas accretion increases the gas fraction to $f_g \sim 1$ and decreases the oxygen abundance due to the gas dilution. Once the star formation rate starts to increase, oxygen is produced by massive stars, and the gas fraction decreases due to the star formation and the outflow.

The present-day oxygen abundance and gas fraction predicted by the model may be roughly consistent with the oxygen abundance of H II regions and the average gas fraction of WLM. We note that nucleosynthesis products by massive stars might be confined to star-forming regions (e.g. Kunth & Sargent 1986), while we assume that the interstellar gas is instantaneously mixed. Also, the degree of the dust depletion and destruction at low metallicities is under debate (e.g. Jackson et al. 2006; Konstantopoulou et al. 2022; Choban et al. 2024).

[4]While the star formation history has been derived under assumption that the metallicity ([Z]) increases with time, we allow chemical abundances to increase and decrease with time. In Fig. 2(d), the chemical abundance and the time do not always show a one-to-one correspondence.

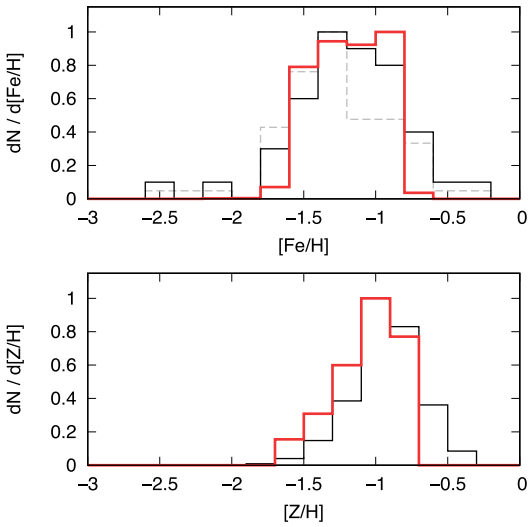

Figure 4. The comparison between the observed and the modelled metallicity distributions. (upper panel) The observed metallicity distribution that includes 44 red giant branch stars in a region on the bar of WLM (black histogram) is compared to a metallicity distribution predicted by the model (red histogram). The grey histogram shows the metallicity distribution that also includes red giant branch stars in the north region of the bar. The observational data are taken from Leaman et al. (2009). (lower panel) The metallicity distribution recovered based on the star formation history (McQuinn et al. 2024, black histogram) is compared to a modelled distribution.

Table 3. Summary of chemical evolution models.

model	sources of elements
A	RMS + LIMS + SNIa + R (NSM + collapsar)
B	no RMS + LIMS + SNIa + R (NSM + collapsar)
C	RMS + LIMS + SNIa + R (NSM)
D	RMS + LIMS + SNIa + R (collapsar)
E	RMS + LIMS + SNIa + no R
F	no RMS + LIMS + SNIa + no R

In Fig. 4, the metallicity distribution of red giant branch stars in a field on the bar (Leaman et al. 2009) and that recovered based on the star formation history (McQuinn et al. 2024) are compared to the model predictions. While the metallicity distribution of red giant branch stars may be composed of a relatively small number of metal-poor stars (Leaman et al. 2009), the average of the red giant branch stars ([Fe/H] $= -1.14$) seems to be almost consistent with the average of the predicted metallicity distribution. Also, the metallicity at the peak of the distribution recovered by McQuinn et al. (2024) is consistent with that predicted by the model.

However, the model tends to predict a small amount of stars of [Fe/H] $\gtrsim -0.8$. Metallicity distributions that include a large number of stars and theoretical models are needed for further discussions.

6 ABUNDANCE RATIOS

To discuss the contribution of astrophysical sources to the chemical evolution, we prepare models that include different astrophysical sources as summarized in Table 3. Physical quantities other than the astrophysical source are not varied among the models.

As well as ejecta from individual events, the temporal variation in the star formation rate and the dilution of the interstellar gas with

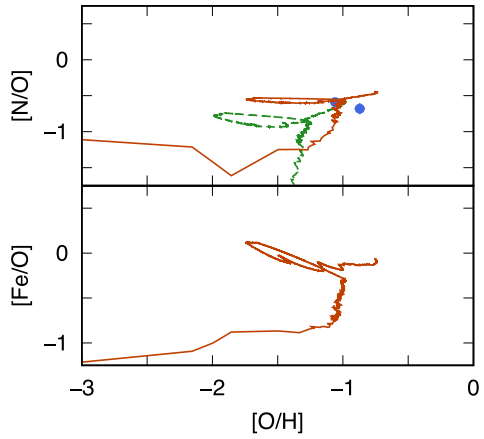

Figure 5. The evolution of [N/O] and [Fe/O] as a function of oxygen abundance. Blue dots in the upper panel show the [N/O] ratio of two H II regions in the bar of WLM. The observational data are taken from Lee et al. (2005). Orange curves show the abundance ratios predicted by model A. For nitrogen, the [N/O] ratio predicted by model B (green curve) is also shown to observe the contribution of rotating massive stars.

the accreting gas seem to influence the evolution of the abundance ratios in Figs 5–7. For instance, a loop seen in the evolution of the abundance ratios results from the variation of the star formation rate and the rate of the gas accretion, such as the gas dilution during a quiescent period and the chemical enrichment in the subsequent star formation episode (e.g. Chiappini, Matteucci & Gratton 1997; Johnson & Weinberg 2020).

In the meanwhile, as discussed in Section 4, the variation of the rate of the gas accretion in quiescent periods is not clear. If the gas dilution in quiescent periods is not significant, the evolution of abundance ratios, including the loops, can be different from that shown in Figs 5–7. Thus, the evolution of the abundance ratios discussed below should be regarded as an example.

6.1 The contribution of astrophysical sources to the chemical evolution

Fig. 5 shows the [N/O] ratio predicted by the model and the ratio of H II regions. The evolution of the [Fe/O] ratio is also shown to discuss the contribution of astrophysical sources that release the nucleosynthesis products on different time-scales.

Rotating massive stars are supposed to produce a large amount of nitrogen compared to non-rotating massive stars at low metallicities (e.g. Meynet & Maeder 2002) and one of the interpretations of the primary-like behaviour of nitrogen of H II regions and stars at low oxygen or iron abundances (e.g. Chiappini et al. 2006; Prantzos et al. 2018; Roy et al. 2021).

The present-day [N/O] ratio predicted by model A seems almost consistent with those of H II regions.[5] Due to the contribution of rotating massive stars, the [N/O] ratio predicted by model A is generally higher than that by model B. Since LIMS contribute to the chemical evolution, the present-day [N/O] ratio predicted by model B is almost comparable to that by model A.

[5]The nitrogen abundance of supergiants tends to be higher than that of H II regions, and this is supposed to be partly due to mixing in the stars (Bresolin et al. 2006, and references therein). In Fig. 5, the present-day [N/O] ratio predicted by the model is compared to the ratio of H II regions.

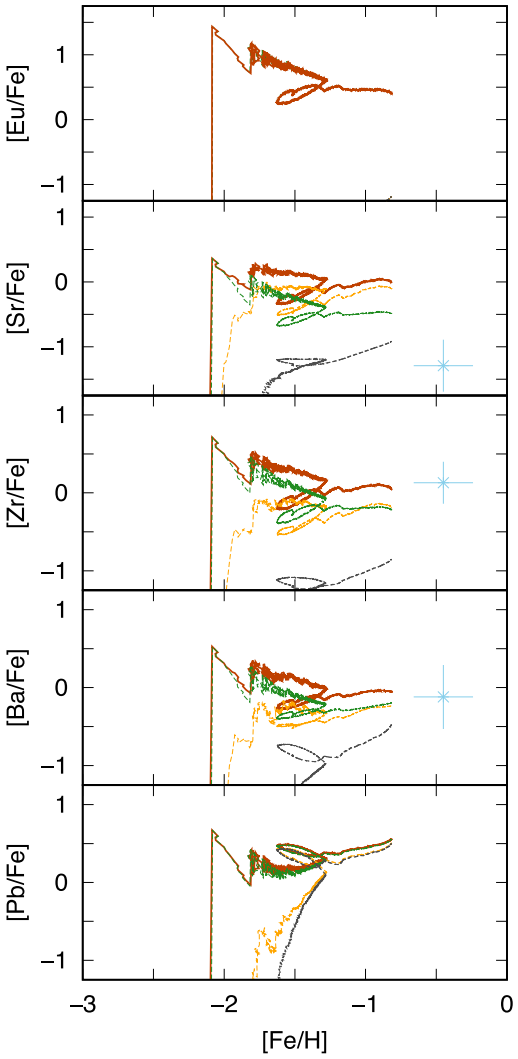

Figure 6. The evolution of [Eu/Fe], [Sr/Fe], [Zr/Fe], [Ba/Fe], and [Pb/Fe] ratios as a function of iron abundance. The asterisks show the abundance ratios of a supergiant (WLM-15). The observational data are taken from Venn et al. (2003). Orange, green, light orange, and grey curves show the abundance ratios predicted by models A, B, E, and F, respectively.

Concerning astrophysical sources, massive asymptotic giant branch (AGB) stars are supposed to produce nitrogen at the stage of the hot bottom burning (e.g. Iben & Renzini 1983, for a review). The relative contribution of astrophysical sources to the nitrogen abundance is an issue to be further discussed.

Compared to the evolution of the [N/O] ratio in the first star formation episode and the subsequent quiescent period, the impact of star formation episodes at later times on the abundance ratio seems less prominent. It might be partly because the ejecta from individual stars are assumed to be instantaneously mixed with the gas in the region.

In the model, iron is produced mainly by massive stars and SNe Ia. Due to the contribution of SNe Ia to the iron abundance, the [Fe/O] ratio continues to increase after the first star formation episode. Once the star formation starts again, the [Fe/O] ratio decreases to [Fe/O] ~ 0 with increasing oxygen abundance. If the oxygen abundance decreases due to the gas dilution, stars of high and low [Fe/O] ratios might be formed at [O/H] ~ -2 to -1.

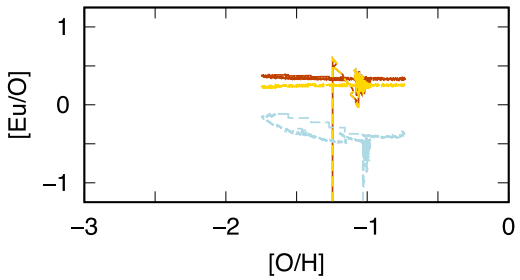

Figure 7. The evolution of [Eu/O] as a function of oxygen abundance. Orange, light blue, and yellow curves show the abundance ratios predicted by models A, C, and D, respectively.

Among trans-iron elements, we focus on Sr, Zr, Ba, Eu, and Pb. Eu is mostly produced by the r-process ($\gtrsim$95 per cent in mass fraction, e.g. Prantzos et al. 2020). The other four elements are representative elements at the first (Sr and Zr), the second (Ba) and the third (Pb) peak of the slow (s-) neutron capture process. These elements are also produced through the r-process.[6]

To discuss the contribution of the s-process and that of the r-process, we compare the evolution of abundance ratios of the trans-iron elements to iron predicted by models A, B, E, and F (Fig. 6). Due to the star formation at the earliest time, the iron abundance rapidly increases to [Fe/H] ~ -1.5 before the first r-process event appears. In addition, the amount of iron released by each massive star is larger than that of trans-iron elements. Although massive stars release the trans-iron elements through winds and supernovae, the impact of the intense star formation may be more important than that of individual events, and the average abundance ratios tend to be low in the earliest phase of the evolution.

The relative contribution to the chemical abundances between the sources of the s-process (LIMS and rotating massive stars) and the r-process candidates is different among the elements. For instance, low mass stars tend to have longer lifetimes and produce heavy s-process elements, such as Ba and Pb, through the main s-process. Thus, the trends in the evolution of the abundance ratios are not always identical.

Currently, there is little observational information that allows us to infer the relative contribution at the early time of the evolution of Local Group dIrrs. Next-generation high-resolution spectrographs on extremely large telescopes may enable to measure the abundance of trans-iron elements of bright old stars, which can provide insights into the source of trans-iron elements and the evolution of dIrrs.

If there are r-process events in the early phase as predicted by the model, the abundance ratios predicted by model E are lower than those by model A, and thus the contribution of the r-process can be large at low iron abundances ([Fe/H] $\lesssim -2$). Also, the abundance ratios predicted by model F suggest that LIMS contribute to the abundance of heavy elements through the s-process.

According to the abundance ratios predicted by models A and B, the contribution of rotating massive stars to the chemical evolution through the weak s-process is clear at [Fe/H] $\gtrsim -1.7$ and greater for lighter trans-iron elements. We note that the evolution of extremely low-metallicity stars and the nucleosynthesis, including the production of trans-iron elements in the environment of high neutron-to-seed ratios, are under debate (e.g. Roberti, Limongi & Chieffi 2024).

The present-day [Zr/Fe] and [Ba/Fe] ratios predicted by model A seem almost consistent with the abundance ratios of the supergiant. The [Sr/Fe] ratio of the supergiant is as low as the ratio predicted by model F. As discussed by Venn et al. (2003, and references therein), the low Sr abundance might be related to the non-local thermodynamic equilibrium effects. The measurement of chemical abundances of individual young and old stars and the information about nucleosynthesis products from stars and r-process candidates will help to discuss the sources of heavy elements in dwarf galaxies of different star formation histories.

6.2 The impact of rare events on the abundance ratios

In Fig. 6, Eu produced by individual r-process events can increase [Eu/Fe], and iron released by stars and SNe Ia in intervals between r-process events can decrease the ratio, resulting in the oscillation. The amplitude seems large at low chemical abundances. The impact of rare r-process events is also seen in abundance ratios of Sr, Zr, Ba, and Pb to iron.

When the star formation rate is low, the number of collapsars tends to decrease. Since both Eu and O abundances are diluted, the [Eu/O] ratio (Fig. 7) predicted by model D is almost constant in the quiescent period after the first star formation episode. On the contrary, the [Eu/O] ratio predicted by model C shows that individual NSMs increase the ratio in the quiescent period, because binary neutron stars reach the explosion with delay. Once the star formation rate starts to increase, the oxygen abundance increases and the [Eu/O] ratio predicted by model C decreases, while NSMs appear and release Eu.

Although the evolution of abundance ratios depends on the astrophysical sources and the yields, when rare events release the nucleosynthesis products on different time-scales, the impact might appear on abundance ratios.

7 SUMMARY

We investigate the chemical evolution in a Local Group dIrr, WLM, with a numerical model where stochasticity is introduced into the occurrence of astrophysical events as rarity. The rate of the outflow and that of the gas accretion are roughly determined by comparing physical quantities of stars and gas to those predicted by the model. We discuss the contribution of astrophysical sources to the chemical evolution.

We estimate the number of astrophysical events in the region on the bar based on the star formation history recovered from the colour–magnitude diagram. Since more massive stars tend to have shorter lifetimes, the time variation of the number of dying massive stars follows that of the star formation rate. Dying LIMS and SNe Ia can appear in quiescent periods between star formation episodes, since they can release the nucleosynthesis products on long time-scales. Due to the low occurrence, the r-process candidates are rare at any time. Collapsars tend to appear when stars are actively formed, and NSMs can also appear in quiescent periods.

The difference in time-scales on which astrophysical sources release heavy elements is reflected in the time variation of the abundance of oxygen and that of iron predicted by the model.

With regard to abundance ratios, the production of nitrogen by rotating massive stars generally increases the [N/O] ratio. Also, lower-mass stars increase the ratio on long time-scales.

Since WLM has an extended star formation history, massive stars are recently and currently formed. The contribution of rotating

[6]Trans-iron elements are also supposed to be produced through the intermediate neutron capture process (Cowan & Rose 1977).

massive stars through the weak s-process is seen at later times in the evolution of abundance ratios of trans-iron elements to iron. Low-mass stars increase the abundance ratios of heavy trans-iron elements to iron through the s-process.

NSMs can release the nucleosynthesis products on long time-scales. Thus, individual NSMs may impact the abundance ratios in quiescent periods between star formation episodes.

ACKNOWLEDGEMENTS

We thank the reviewer for comments and questions. Calculations in this article have been carried out on PC cluster at the Center for Computational Astrophysics, NAOJ.

DATA AVAILABILITY

No new data were generated or analysed in support of this research.

REFERENCES

Albers S. M. et al., 2019, MNRAS, 490, 5538
Athanassoula E., 1992, MNRAS, 259, 345
Barnes D. G., de Blok W. J. G., 2004, MNRAS, 351, 333
Beniamini P., Piran T., 2019, MNRAS, 487, 4847
Bradamante F., Matteucci F., D'Ercole A., 1998, A&A, 337, 338
Bresolin F., Pietrzyński G., Urbaneja M. A., Gieren W., Kudritzki R.-P., Venn K. A., 2006, ApJ, 648, 1007
Chiappini C., Matteucci F., Gratton R., 1997, ApJ, 477, 765
Chiappini C., Hirschi R., Meynet G., Ekström S., Maeder A., Matteucci F., 2006, A&A, 449, L27
Choban C. R., Kereš D., Sandstrom K. M., Hopkins P. F., Hayward C. C., Faucher-Giguère C.-A., 2024, MNRAS, 529, 2356
Cowan J. J., Rose W. K., 1977, ApJ, 212, 149
Cristallo S., Straniero O., Piersanti L., Gobrecht D., 2015, ApJS, 219, 40
de los Reyes M. A. C., Kennicutt R. C., 2019, ApJ, 872, 16
Diehl R., Prantzos N., 2023, preprint (arXiv:2303.01825)
Dolphin A. E., 2000, ApJ, 531, 804
Elmegreen B. G., Rubio M., Hunter D. A., Verdugo C., Brinks E., Schruba A., 2013, Nature, 495, 487
Fukagawa N., Prantzos N., 2023, MNRAS, 524, 4688
Gerola H., Seiden P. E., Schulman L. S., 1980, ApJ, 242, 517
Gilmore G., Wyse R. F. G., 1991, ApJ, 367, L55
Greggio L., 2005, A&A, 441, 1055
Hartwick F. D. A., 1976, ApJ, 209, 418
Iben I., Renzini A., 1983, ARA&A, 21, 271
Iwamoto K., Brachwitz F., Nomoto K., Kishimoto N., Umeda H., Hix W. R., Thielemann F.-K., 1999, ApJS, 125, 439
Jackson D. C., Skillman E. D., Cannon J. M., Côté S., 2004, AJ, 128, 1219
Jackson D. C., Cannon J. M., Skillman E. D., Lee H., Gehrz R. D., Woodward C. E., Polomski E., 2006, ApJ, 646, 192
Johnson J. W., Weinberg D. H., 2020, MNRAS, 498, 1364
Kepley A. A., Wilcots E. M., Hunter D. A., Nordgren T., 2007, AJ, 133, 2242
Konstantopoulou C. et al., 2022, A&A, 666, A12
Kroupa P., 2002, ASPC, 285, 86
Kunth D., Sargent W. L. W., 1986, ApJ, 300, 496
Larson R. B., 1974, MNRAS, 169, 229
Leaman R., Cole A. A., Venn K. A., Tolstoy E., Irwin M. J., Szeifert T., Skillman E. D., McConnachie1 A. W., 2009, ApJ, 699, 1
Leaman R. et al., 2012, ApJ, 750, 33
Lee H., Skillman E. D., Venn K. A., 2005, ApJ, 620, 223
Limongi M., Chieffi A., 2018, ApJS, 237, 13
Lodders K., Palme H., Gail H.-P., 2009, Landolt-Börnstein, New series, VI/4B, 560
Lynden-Bell D., 1975, VA, 19, 299
MacFadyen A. I., Woosley S. E., 1999, ApJ, 524, 262
Maoz D., Graur O., 2017, ApJ, 848, 25
Marconi G., Tosi M., Greggio L., Focardi P., 1995, AJ, 109, 173
Matteucci F., 2021, A&ARv, 29, 5
Matteucci F., Chiosi C., 1983, A&A, 123, 121
McConnachie A. W., 2012, AJ, 144, 4
McQuinn K. B. W. et al., 2024, ApJ, 961, 16
Meynet G., Maeder A., 2002, A&A, 390, 561
Muratov A. L., Kereš D., Faucher-Giguère C.-A., Hopkins P. F., Quataert E., Murray N., 2015, MNRAS, 454, 2691
Pilyugin L. S., 1992, A&A, 260, 58
Prantzos N., Abia C., Limongi M., Chieffi A., Cristallo S., 2018, MNRAS, 476, 3432
Prantzos N., Abia C., Cristallo S., Limongi M., Chieffi A., 2020, MNRAS, 491, 1832
Roberti L., Limongi M., Chieffi A., 2024, ApJS, 270, 28
Roy A., Dopita M. A., Krumholz M. R., Kewley L. J., Sutherland R. S., Heger A., 2021, MNRAS, 502, 4359
Sánchez Almeida J. et al., 2015, ApJ, 810, L15
Schaller G., Schaerer D., Meynet G., Maeder A., 1992, A&AS, 96, 269
Searle L., Sargent W. L. W., Bagnuolo W. G., 1973, ApJ, 179, 427
Skillman E. D., Terlevich R., Melnick J., 1989, MNRAS, 240, 563
Tinsley B. M., 1979, ApJ, 229, 1046
Tosi M., Greggio L., Focardi P., 1989, Ap&SS, 156, 295
Umeda H., Nomoto K., 2002, ApJ, 565, 385
Urbaneja M. A., Kudritzki R.-P., Bresolin F., Przybilla N., Gieren W., Pietrzyński G., 2008, ApJ, 684, 118
van de Voort F., 2017, ASSL, 430, 301
Venn K. A., Tolstoy E., Kaufer A., Skillman E. D., Clarkson S. M., Smartt S. J., Lennon D. J., Kudritzki R. P., 2003, AJ, 126, 1326
Whiting A. B., Hau G. K. T., Irwin M., 1999, AJ, 118, 2767
Woo J., Courteau S., Dekel A., 2008, MNRAS, 390, 1453

This paper has been typeset from a TEX/LATEX file prepared by the author.